JCI The Journal of Clinical Investigation

MicroRNA-155 promotes atherosclerosis by repressing *Bcl6* in macrophages

Maliheh Nazari-Jahantigh, … , Christian Weber, Andreas Schober

J Clin Invest. 2012;122(11):4190-4202. https://doi.org/10.1172/JCI61716.

Research Article **Cardiology**

Macrophages in atherosclerotic plaques drive inflammatory responses, degrade lipoproteins, and phagocytose dead cells. MicroRNAs (miRs) control the differentiation and activity of macrophages by regulating the signaling of key transcription factors. However, the functional role of macrophage-related miRs in the immune response during atherogenesis is unknown. Here, we report that miR-155 is specifically expressed in atherosclerotic plaques and proinflammatory macrophages, where it was induced by treatment with mildly oxidized LDL (moxLDL) and IFN-γ. Leukocyte-specific *Mir155* deficiency reduced plaque size and number of lesional macrophages after partial carotid ligation in atherosclerotic (*Apoe*$^{-/-}$) mice. In macrophages stimulated with moxLDL/IFN-γ in vitro, and in lesional macrophages, loss of *Mir155* reduced the expression of the chemokine CCL2, which promotes the recruitment of monocytes to atherosclerotic plaques. Additionally, we found that miR-155 directly repressed expression of BCL6, a transcription factor that attenuates proinflammatory NF-κB signaling. Silencing of *Bcl6* in mice harboring *Mir155*$^{-/-}$ macrophages enhanced plaque formation and CCL2 expression. Taken together, these data demonstrated that miR-155 plays a key role in atherogenic programming of macrophages to sustain and enhance vascular inflammation.

MicroRNA-155 promotes atherosclerosis by repressing *Bcl6* in macrophages

Maliheh Nazari-Jahantigh,[1,2] Yuanyuan Wei,[1,2] Heidi Noels,[2] Shamima Akhtar,[2] Zhe Zhou,[2] Rory R. Koenen,[1,3] Kathrin Heyll,[1,2] Felix Gremse,[4] Fabian Kiessling,[4] Jochen Grommes,[5] Christian Weber,[1,3,6] and Andreas Schober[1,2]

[1]Institute for Cardiovascular Prevention, Ludwig-Maximilians-University Munich, Munich, Germany. [2]Institute for Molecular Cardiovascular Research, RWTH Aachen University, Aachen, Germany. [3]Cardiovascular Research Institute Maastricht, University Maastricht, Maastricht, The Netherlands. [4]Department of Experimental Molecular Imaging, RWTH Aachen University, Aachen, Germany. [5]European Vascular Center Aachen-Maastricht, RWTH Aachen University and Medical University Maastricht, Maastricht, The Netherlands. [6]Munich Heart Alliance, Munich, Germany.

Macrophages in atherosclerotic plaques drive inflammatory responses, degrade lipoproteins, and phagocytose dead cells. MicroRNAs (miRs) control the differentiation and activity of macrophages by regulating the signaling of key transcription factors. However, the functional role of macrophage-related miRs in the immune response during atherogenesis is unknown. Here, we report that miR-155 is specifically expressed in atherosclerotic plaques and proinflammatory macrophages, where it was induced by treatment with mildly oxidized LDL (moxLDL) and IFN-γ. Leukocyte-specific *Mir155* deficiency reduced plaque size and number of lesional macrophages after partial carotid ligation in atherosclerotic (*Apoe*$^{-/-}$) mice. In macrophages stimulated with moxLDL/IFN-γ in vitro, and in lesional macrophages, loss of *Mir155* reduced the expression of the chemokine CCL2, which promotes the recruitment of monocytes to atherosclerotic plaques. Additionally, we found that miR-155 directly repressed expression of BCL6, a transcription factor that attenuates proinflammatory NF-κB signaling. Silencing of *Bcl6* in mice harboring *Mir155*$^{-/-}$ macrophages enhanced plaque formation and CCL2 expression. Taken together, these data demonstrated that miR-155 plays a key role in atherogenic programming of macrophages to sustain and enhance vascular inflammation.

Introduction

Macrophages are the principal effector cells in atherosclerosis, in which they perpetuate the vascular inflammatory response to lipid overloading (1, 2). The subendothelial deposition of lipoproteins precedes infiltration by macrophages, which take up modified lipoproteins in an unrestricted manner via scavenger receptors (2). The lysosomal degradation of lipoproteins generates free cholesterol, which is then converted to, and stored as, cholesterol esters (1). Macrophages can dispose of cholesterol by reverse transport to the liver through several mechanisms of HDL-mediated cholesterol efflux (3, 4). In atherosclerosis, the influx of lipoproteins into macrophages exceeds cholesterol efflux, resulting in the intracellular accumulation of cholesterol esters within lipid droplets, a hallmark of macrophage-derived foam cells (5). Although lipid-handling macrophages show an antiinflammatory phenotype characterized by activation of PPARγ and NR1H3/NR1H2, excessive intracellular lipid storage can induce inflammatory activation by increasing free cholesterol or by inducing the formation of cholesterol crystals (6–10). Conversely, stimulation with inflammatory mediators (such as TNF-α, IL-1β, or the Th1 cytokine IFN-γ) and activation of TLR4 (e.g., by minimally modified lipoproteins) not only induces an inflammatory response, but also enhances intracellular lipid accumulation in macrophages (11, 12). NF-κB–dependent signaling pathways are of crucial importance in the proinflammatory activation of macrophages; however, in vivo studies on the role of the myeloid NF-κB module in atherosclerosis show inconsistent results, indicative of the complexity of the different NF-κB signaling pathways that control both the activation and the resolution phases of inflammation (13–15). Genetic deficiency of TLR4 or its downstream signaling molecule, MYD88, both of which are potent activators of classical NF-κB signaling, limits atherosclerosis by reducing macrophage recruitment and is also associated with reduced expression of chemokines, such as CCL2 (16, 17). In atherosclerosis, macrophage-derived CCL2 acts in concert with endothelial CXCL1 to induce additional macrophage accumulation through a positive feedback regulatory mechanism (18, 19).

BCL6 is primarily expressed in B cells during the germinal center phase of differentiation and acts as a proto-oncogene in diffuse larger B cell lymphomas by compromising the cells' ability to sense DNA damage (20). The effect of BCL6, at least in part, on the germinal center reaction is mediated by counter-regulation of NF-κB activation (20). Several mechanisms of BCL6-mediated inhibition of NF-κB signaling have been described, including direct repression of p50, inhibitory binding of BCL6 to NF-κB proteins, and opposing regulation of NF-κB target genes (21–24). In macrophages, *Bcl6* is transiently induced in a NF-κB–dependent manner and directly represses *Ccl2* expression, which indicates that BCL6 inhibits the acute inflammatory response (23, 24).

MicroRNAs (miRs) play an important role in macrophage biology by regulating their differentiation from precursor cells and modifying their inflammatory capacity (25). The typical effect of an individual miR lowers the protein level by less than 2-fold, primarily by destabilizing the target mRNA (26). However, an miR can effectively control the function of its target, either by switch or by fine-tuning interactions (27). In macrophages, functional polarization is associated with the upregulation of a distinct set of miRs (28, 29). TLR4-mediated activation of NF-κB induces a negative feedback loop by upregulating miRs such as miR-21, miR-147, miR-210, miR-34a, and miR-146, which dampen TLR-induced signaling and cytokine expression (30–32). In contrast, miR-155

Conflict of interest: The authors have declared that no conflict of interest exists.
Citation for this article: *J Clin Invest.* 2012;122(11):4190–4202. doi:10.1172/JCI61716.

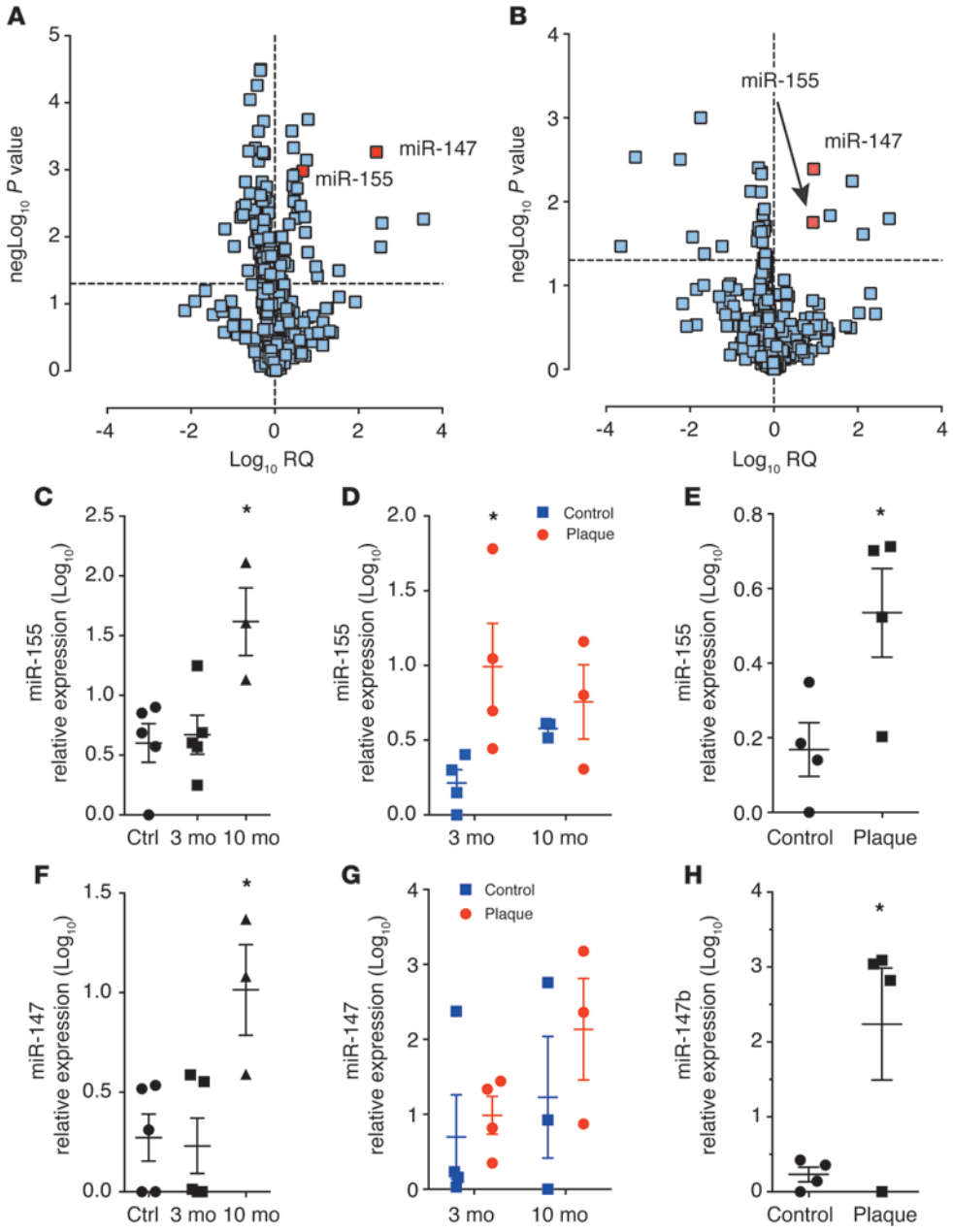

Figure 1
Expression of miR-155 and miR-147 in atherosclerotic lesions and in inflammatory macrophages. (**A**) Expression profile of miRs in carotid plaques from *Apoe*$^{-/-}$ mice 6 weeks after partial ligation in the contralateral carotid artery (n = 6). (**B**) Expression profile of miRs in LPS- and IFN-γ–stimulated and unstimulated BMDMs (n = 5). (**C** and **F**) Expression of miR-155 (**C**) and miR-147 (**F**) in the aortic vessel wall of *Apoe*$^{-/-}$ mice fed regular diet (ctrl) or HFD for 3 or 10 months (n = 3–5 per group). *P < 0.05 vs. ctrl and 3 months. (**D** and **G**) Expression of miR-155 (**D**) and miR-147 (**G**) in plaque samples laser-microdissected from the aortic root of *Apoe*$^{-/-}$ mice fed HFD for 3 or 10 months (n = 3–4 per group). The miR expression profile of these plaques was compared with that in samples from arteries without plaques within the same mouse (control). *P < 0.05 vs. control. (**E** and **H**) Expression of miR-155 (**E**) and miR-147b (the human homolog of mouse miR-147; **H**) in human carotid plaque samples and vessel walls (control). n = 3–4 per group. *P < 0.05. Data represent mean (**A** and **B**) or mean ± SEM (**C**–**H**).

shows both anti- and proinflammatory effects by regulating TAB2 and SOCS1, respectively (29, 32, 33). Furthermore, upregulation of miR-29b and miR-125a-5p in inflammatory macrophages promotes the expression of proinflammatory cytokines, suggestive of feed-forward regulation (29). Interestingly, treatment of macrophages with oxidized LDL (oxLDL) appears to suppress several miRs induced after inflammatory stimulation, such as miR-146a, miR-155, and miR-21 (34, 35). oxLDL-mediated downregulation of miR-146a enhances both lipid uptake and TLR4 signaling (34). However, oxLDL can also upregulate miR-125a-5p and miR-155, which reduce the accumulation of lipids and cytokine secretion in macrophages (36, 37). miRs that are crucial for the inflammatory macrophage response, such as miR-21, miR-210, miR-146a, miR-34a, miR-147, and miR-125a-5p, are significantly upregulated in human atherosclerotic lesions, which indicates that macrophage-derived miRs contribute to atherogenesis (38, 39). In addition, miR-33 promotes the progression of atherosclerosis and impairs ABCA1-dependent cholesterol removal from lesional macrophages (40). Although these data suggest that miRs play a key role in regulating macrophage function at the intersection of lipid-handling and inflammatory activation, it is still unclear how miRs affect macrophages in atherosclerosis.

Here, we found that miR-155 was upregulated in inflammatory macrophages and in macrophages in atherosclerotic lesions. Increased expression of miR-155 induced CCL2 in macrophages stimulated with mildly oxLDL (moxLDL) and IFN-γ via direct suppression of *Bcl6*, a transcription factor that counter-regulates NF-κB activation. Furthermore, we demonstrated that deficiency of *Mir155* in hematopoietic cells reduced advanced atherosclerotic plaque formation and decreased CCL2 expression in lesional

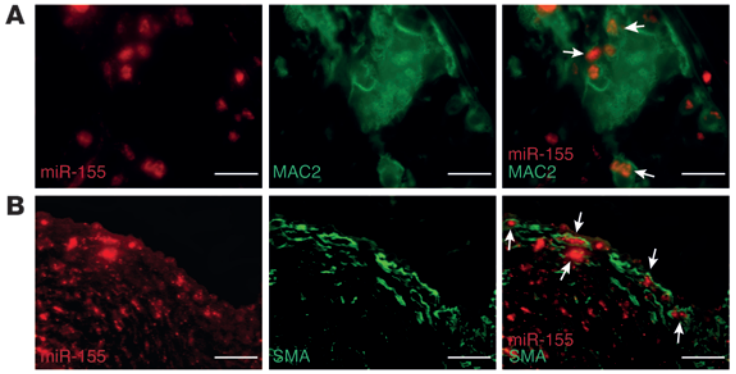

Figure 2
miR-155 is expressed in macrophages and SMCs in atherosclerotic lesions. (**A**) In situ hybridization for miR-155 (red) and immunostaining for galectin-3 (MAC2; green) was performed in murine carotid artery plaques. Arrows denote macrophages expressing miR-155. (**B**) In situ hybridization for miR-155 (red) and immunostaining for SMA (green) was performed in murine carotid artery plaques. Arrows denote SMCs expressing miR-155. Scale bars: 20 μm.

macrophages by derepressing *Bcl6*. In summary, we identified what we believe to be a novel miR-155–dependent inflammatory pathway in macrophages that plays a role in atherosclerosis.

Results

MiR expression profile in atherosclerosis and inflammatory macrophages. To study the miR expression signature in atherosclerosis, flow-mediated plaque formation was induced in *Apoe*$^{-/-}$ mice by partial carotid ligation (41). When combined with high-fat diet (HFD) feeding, this process resulted in advanced stenotic plaques within 6 weeks, as detected by micro–computed tomography (42) and immunostaining (Supplemental Figure 1; supplemental material available online with this article; doi:10.1172/JCI61716DS1). We found that 33 miRs, including miR-155 and miR-147, were increased, and 83 miRs were decreased, in carotid arteries with plaques versus those without (Figure 1A and Supplemental Tables 1 and 2). Notably, miR-155 and miR-147 were also among the 6 upregulated miRs identified in BM-derived macrophages (BMDMs) after stimulation with LPS and IFN-γ compared with unstimulated BMDMs (Figure 1B and Supplemental Table 3). Moreover, stimulation with LPS and IFN-γ suppressed the expression of 26 miRs in BMDMs (Figure 1B and Supplemental Table 4).

To further study the role of miR-155 and miR-147 expression during atherosclerosis, we quantified their expression in a mouse model of diet-induced atherosclerosis. Expression of miR-155 in the aortic wall of *Apoe*$^{-/-}$ mice was significantly higher after 10 months of HFD feeding than after 3 months of HFD or regular chow diet (P = 0.0111; Figure 1C). However, miR-155 expression in plaque samples of *Apoe*$^{-/-}$ mice was already increased after 3 months of HFD feeding compared with that in the normal arterial wall (Figure 1D). Expression of miR-155 was also higher in human carotid plaques than in the artery wall (Figure 1E). Similar to miR-155, expression of miR-147 in the murine aortic wall only increased after 10 months of HFD feeding (Figure 1F). Although miR-147 expression was not significantly increased in murine plaques (P = 0.6161 at 3 months and P = 0.3567 at 10 months; Figure 1G), the expression of miR-147b — the human homolog of murine miR-147 — was increased in human carotid plaques compared with that in the vessel wall (Figure 1H). Thus, upregulation of miR-155 was consistently observed in different mouse models of atherosclerosis and in human plaques, whereas miR-147 expression was more variable.

Macrophages play a key role in the inflammatory response during atherosclerosis, and M1 polarized macrophages have been described in atherosclerotic lesions. Therefore, we performed in situ hybridization to identify the cellular source of miR-155 in atherosclerotic lesions. First, we verified the specificity of in situ hybridization for miR-155 using *Mir155*$^{-/-}$ mice as negative controls (Supplemental Figure 2). In atherosclerotic lesions, additional immunostaining for the macrophage marker MAC2 demonstrated that the majority of lesional macrophages expressed miR-155 (Figure 2A). Additionally, some SMCs also expressed miR-155, as detected by combined immunostaining for miR-155 and SMA (Figure 2B). Therefore, both hematopoietic and vessel wall–derived cells in atherosclerotic lesions expressed miR-155.

Effect of miR-155 on atherosclerosis. To study the function of miR-155 in atherogenesis, partial carotid ligation was performed in *Mir155*$^{+/+}$*Apoe*$^{-/-}$ mice transplanted with *Mir155*$^{-/-}$*Apoe*$^{-/-}$ BM cells and in *Mir155*$^{-/-}$*Apoe*$^{-/-}$ mice transplanted with *Mir155*$^{+/+}$*Apoe*$^{-/-}$ BM. *Mir155*$^{+/+}$*Apoe*$^{-/-}$ mice repopulated with *Mir155*$^{+/+}$*Apoe*$^{-/-}$ BM cells were used as controls. A significant reduction in plaque size and in the number of macrophages per plaque was found in *Mir155*$^{+/+}$*Apoe*$^{-/-}$ mice harboring *Mir155*$^{-/-}$*Apoe*$^{-/-}$ BM compared with the other 2 experimental groups (Figure 3, A and B). However, the medial area, external elastic lamina length, relative macrophage plaque content (determined as macrophage number or MAC2$^+$ area normalized to the plaque area), and macrophage size were not different among the groups (Figure 3A and Supplemental Figures 3 and 4). Moreover, the relative SMC content tended to be decreased in *Mir155*$^{+/+}$*Apoe*$^{-/-}$ mice harboring *Mir155*$^{-/-}$*Apoe*$^{-/-}$ BM (Figure 3C), whereas the relative lesional CD3$^+$ T cell and MPO$^+$ neutrophil counts and the collagen type I content were not substantially affected by *Mir155* deficiency (Figure 3, D–F). The number of apoptotic macrophages in the lesions was similar in all 3 groups (Figure 3G). No differences were observed in the serum lipoprotein profile among the groups (Supplemental Figure 5). A combination of immunostaining for MAC2 and Oil red O staining demonstrated that lipid accumulation in *Mir155*$^{-/-}$ macrophages in atherosclerotic lesions was significantly less than that in *Mir155*$^{+/+}$ macrophages (P = 0.0466; Supplemental Figure 6). These results indicate that the expression of miR-155 in lesional macrophages promotes atherosclerosis by increasing the number of lesional macrophages and critically regulating their function.

Role of miR-155 in proinflammatory macrophage activation. miR-155 is implicated in the regulation of proinflammatory M1 macrophage polarization (43); however, its functional role in the development of atherosclerotic plaque containing activated macrophages is unclear. Our analysis of macrophage-specific miR-155 expression, which was downregulated during macrophage differentiation (Figure 4A), showed that polarization of BMDMs into proinflammatory M1-type macrophages upon stimulation with LPS and IFN-γ (in contrast to antiinflammatory M2-type polarization induced by IL-4) induced miR-155 expression (Figure 4B). Native LDL and moxLDL slightly increased miR-155 expression, whereas highly oxLDL reduced the expression of miR-155 (Figure 4B)

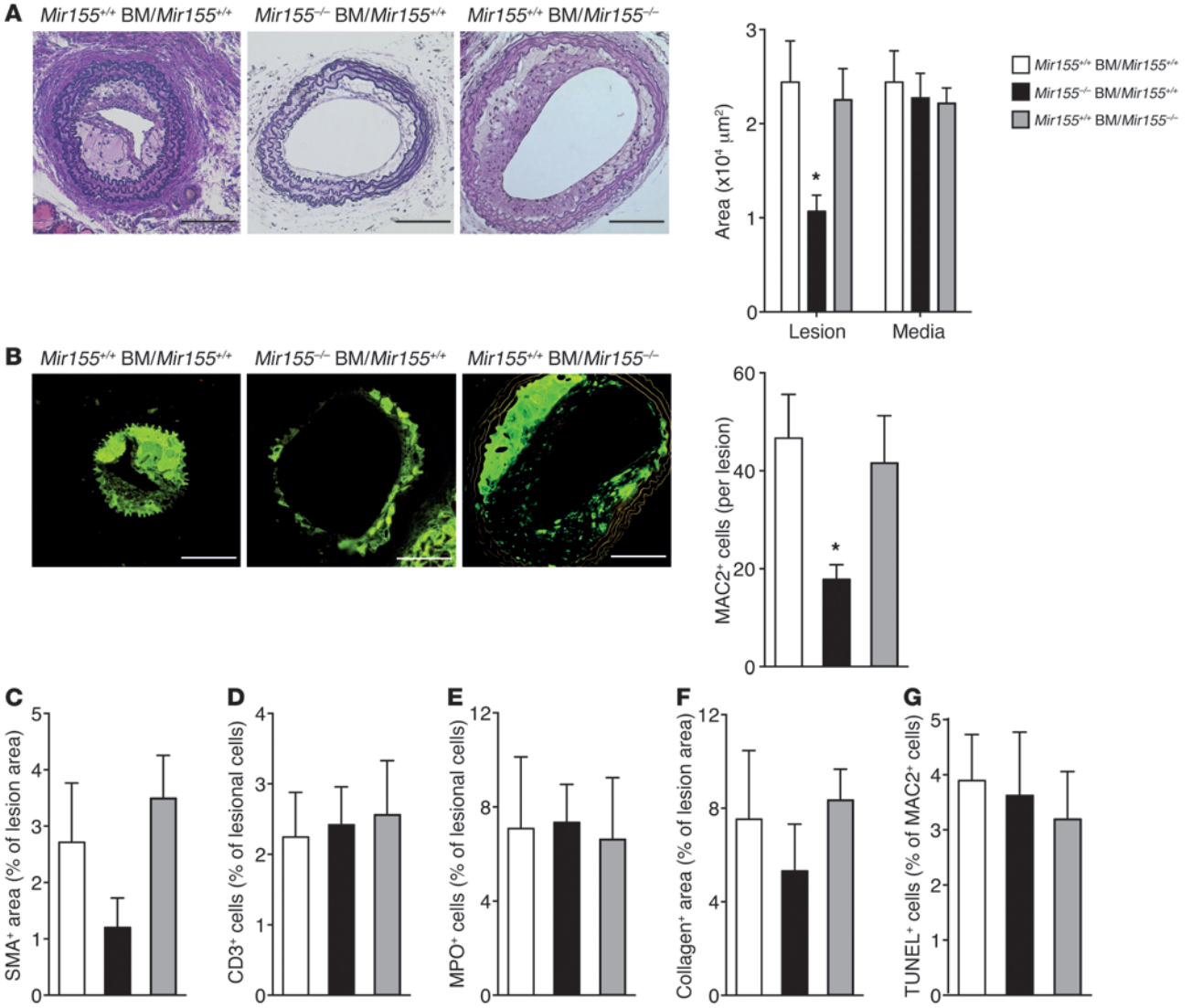

Figure 3

Role of miR-155 in atherosclerosis. (**A**) Lesion area and medial area 6 weeks after partial carotid ligation in *Mir155*$^{+/+}$*Apoe*$^{-/-}$ mice harboring *Mir155*$^{+/+}$*Apoe*$^{-/-}$ or *Mir155*$^{-/-}$*Apoe*$^{-/-}$ BM (*Mir155*$^{+/+}$ BM/*Mir155*$^{+/+}$ [*n* = 7] and *Mir155*$^{-/-}$ BM/*Mir155*$^{+/+}$ [*n* = 8] respectively) and in *Mir155*$^{-/-}$*Apoe*$^{-/-}$ mice harboring *Mir155*$^{+/+}$*Apoe*$^{-/-}$ BM (*Mir155*$^{+/+}$ BM/*Mir155*$^{-/-}$ [*n* = 6]). Representative images are shown. (**B**) The number of MAC2^{+} macrophages in carotid lesions was determined by immunostaining. Representative images are shown. (**C**–**F**) Lesional content of SMCs, T cells, neutrophils, and collagen, assessed by immunostaining for SMA (**C**), CD3 (**D**), MPO (**E**), and collagen type I (**F**). (**G**) Apoptotic macrophages were quantified in carotid lesions by combined TUNEL staining and MAC2 immunostaining. *n* = 6–8 mice per group. **P* < 0.05. Scale bars: 100 μM. Data are mean ± SEM.

and induced expression of the M2 marker *Mrc1* (Supplemental Figure 7). This indicates that the degree of LDL oxidation plays a role in the effect of modified LDL on miR-155 expression. Similar to LPS and IFN-γ, stimulation with moxLDL and IFN-γ induced miR-155 together with M1-type markers, such as *Nos2* and *Tnf* (Figure 4B and Supplemental Figure 7). Thus, moxLDL-stimulated macrophages also required IFN-γ, which is highly expressed in atherosclerotic plaques (44), to develop a M1 phenotype and to substantially upregulate miR-155 expression. In contrast to moxLDL- and IFN-γ–stimulated *Mir155*$^{+/+}$ BMDMs, *Mir155*$^{-/-}$ BMDMs mainly showed reduced expression of *Ccl2* mRNA (and also some reduction in *Tnf* mRNA), whereas no substantial difference in *Il1b* and *Nos2* expression was detectable between *Mir155*$^{+/+}$ and *Mir155*$^{-/-}$ BMDMs (Figure 4C). The effect of miR-155 on CCL2 expression and secretion was confirmed at the protein level (Figure 4, D and E). In contrast, macrophage migration and apoptosis appeared to be unchanged in the absence of miR-155 in vitro (Figure 4, F and G). To study the effect of miR-155 on CCL2 expression in lesional macrophages, combined immunostaining for CCL2 and MAC2 was performed (Figure 5). In line with the results obtained for BMDMs, the number of CCL2-expressing macrophages was substantially reduced in carotid lesions in *Mir155*$^{+/+}$*Apoe*$^{-/-}$ mice harboring *Mir155*$^{-/-}$*Apoe*$^{-/-}$ BM compared with that in *Mir155*$^{+/+}$*Apoe*$^{-/-}$ and *Mir155*$^{-/-}$*Apoe*$^{-/-}$ mice harboring *Mir155*$^{+/+}$*Apoe*$^{-/-}$ BM (Figure 5), which may lead to impaired macrophage infiltration into the plaques in *Apoe*$^{-/-}$ mice with *Mir155*-deficient leukocytes.

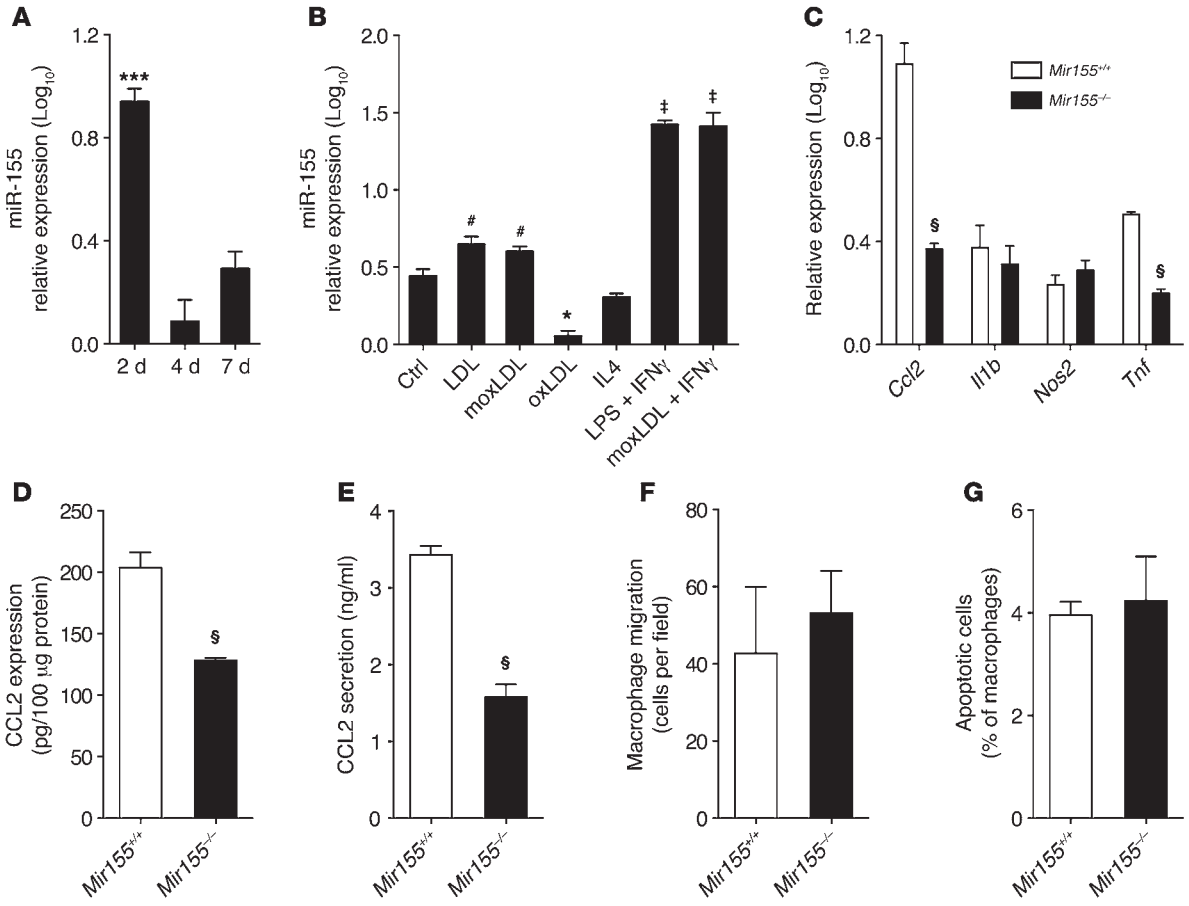

Figure 4

Role of miR-155 in atherogenic macrophage activation. (**A**) miR-155 expression by quantitative RT-PCR in murine BM cells cultured in L929-conditioned medium to induce macrophage differentiation. (**B**) Regulation of miR-155 expression in BMDMs by modified LDL was quantified and compared with classical and alternative macrophage activation by quantitative RT-PCR. (**C**) Expression of inflammatory macrophage markers was analyzed by quantitative RT-PCR in BMDMs from *Mir155*$^{+/+}$ and *Mir155*$^{-/-}$ mice after stimulation with moxLDL and IFN-γ. (**D** and **E**) CCL2 protein in cell lysates (**D**) and in the cell culture medium (**E**) of BMDMs from *Mir155*$^{+/+}$ and *Mir155*$^{-/-}$ mice after stimulation with moxLDL and IFN-γ, quantified by ELISA. (**F**) Migration of *Mir155*$^{+/+}$ and *Mir155*$^{-/-}$ BMDMs across a Transwell filter toward CCL2. (**G**) Apoptosis of BMDMs from *Mir155*$^{+/+}$ and *Mir155*$^{-/-}$ mice, determined by TUNEL assay. $^{*}P < 0.05$, $^{***}P < 0.001$ vs. all other groups; $^{\#}P < 0.05$ vs. control, oxLDL, IL-4, LPS plus IFN-γ, and moxLDL plus IFN-γ; $^{\ddagger}P < 0.05$ vs. control, native LDL, moxLDL, oxLDL, and IL-4; $^{\S}P < 0.05$ vs. *Mir155*$^{+/+}$. 3 independent experiments were conducted per group. Data are mean ± SEM.

Mechanism of miR-155–mediated cytokine expression. Several targets for miR-155 have been described in macrophages, including *Socs1* and *Sfpi1*, which regulate inflammatory and developmental processes, respectively (33, 45). To identify the mechanism of miR-155–induced CCL2 expression, we studied 7 potential miR-155 targets that were increased in either unstimulated *Mir155*$^{-/-}$ BMDMs or in *Mir155*$^{-/-}$ BMDMs stimulated with moxLDL and IFN-γ (Figure 6, A and B) using EIF2C2-specific IP. miR-155 was highly enriched in EIF2C2-containing miR-induced silencing complexes (mRISCs) in *Mir155*$^{+/+}$, but not *Mir155*$^{-/-}$, BMDMs (Figure 6C). Of the 7 potential miR-155 targets in BMDMs, *Rela*, *Tcf7l2*, *Socs1*, *Bcl6*, and *Sfpi1* were associated with EIF2C2 in *Mir155*$^{+/+}$, but not *Mir155*$^{-/-}$, BMDMs (Figure 6D and Supplemental Figure 8), indicative of direct repression by miR-155, in moxLDL- and IFN-γ–stimulated macrophages. Although 2 binding sites for miR-155 are predicted to reside within the 3′UTR of *Bcl6*, to our knowledge, targeting *Bcl6* has not been described previously. Therefore, using luciferase reporter assays, we verified the direct targeting of the 3′UTR of *Bcl6* by miR-155 (Figure 6, E and F). Mutation of one of the predicted binding sites within the *Bcl6* 3′UTR prevented suppression by miR-155 (Figure 6F).

To study which miR-155 target regulates expression of *Ccl2* and *Tnf*, silencing of *Socs1*, *Bcl6*, and *Sfpi1* was performed using RNA interference (Supplemental Figure 9). Silencing *Bcl6*, but not *Socs1* or *Sfpi1*, increased *Ccl2* and *Tnf* mRNA expression in *Mir155*$^{-/-}$ BMDMs (Figure 7 and Supplemental Figure 10). Upregulation of CCL2 in *Mir155*$^{-/-}$ BMDMs by *Bcl6*-specific siRNA was confirmed at the protein level, whereas TNF-α protein levels only showed a tendency toward an increase after *Bcl6* siRNA treatment (Figure 7). Thus, derepression of the miR-155 target *Bcl6* in *Mir155*$^{-/-}$ macrophages reduced atherogenic cytokine expression.

Regulation of the antiinflammatory role of BCL6 in atherogenic macrophages. BCL6 acts as an NF-κB antagonist either by opposing the upregulation of many NF-κB–responsive target genes in stimulated macrophages or by directly inhibiting NF-κB activity (22, 23, 46). We found that blocking NF-κB activation using the NF-κB inhibi-

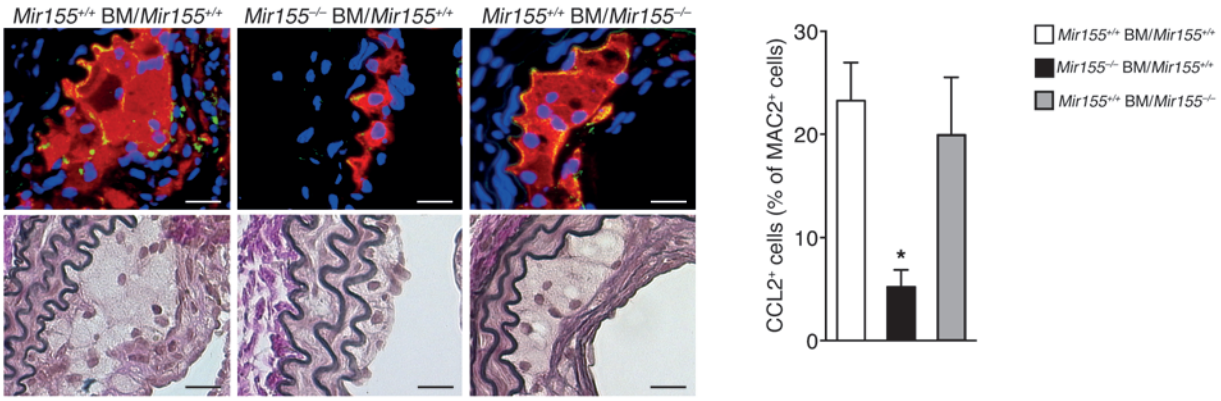

Figure 5
Role of miR-155 in CCL2 expression by lesional macrophages. Expression of CCL2 (green) was assessed in MAC2+ macrophages (red) from plaques 6 weeks after partial carotid ligation in *Apoe*$^{-/-}$ mice harboring *Mir155*$^{+/+}$*Apoe*$^{-/-}$ or *Mir155*$^{-/-}$*Apoe*$^{-/-}$ BM and in *Mir155*$^{-/-}$*Apoe*$^{-/-}$ mice harboring *Mir155*$^{+/+}$*Apoe*$^{-/-}$ BM by double immunostaining. Representative overlays of CCL2 and MAC2 immunostaining are shown (top). CCL2 expressed in macrophages is shown in yellow. The percentage of CCL2+ macrophages was determined. Adjacent sections were stained with EVG to demonstrate lesion morphology (bottom). n = 6–8 per group. *P < 0.05. Scale bars: 20 μm. Data are mean ± SEM.

tor BAY11-7985 reduced *Ccl2* and *Tnf* mRNA expression in *Bcl6* siRNA–treated *Mir155*$^{-/-}$ macrophages (Figure 8, A and B). To determine whether autocrine stimulation by TNF-α contributes to the effect of miR-155 on CCL2 expression, TNF-α in the cell culture medium was blocked using an anti–TNF-α antibody. Although the antibody inhibited CCL2 secretion by *Mir155*$^{+/+}$ macrophages, blocking TNF-α did not abrogate the reduced CCL2 secretion in *Mir155*$^{-/-}$ BMDMs compared with *Mir155*$^{+/+}$ macrophages (Figure 8, C and D), which indicates that miR-155 increases CCL2 secretion independently of elevated *Tnf* expression. In contrast to *Mir155*$^{-/-}$ macrophages, *Bcl6* mRNA in *Mir155*$^{+/+}$ macrophages was upregulated 24 hours after stimulation with moxLDL and IFN-γ, reducing the difference in *Bcl6* expression between unstimulated *Mir155*$^{+/+}$ and *Mir155*$^{-/-}$ macrophages (Figure 8E). Similar results were obtained at the protein level (Figure 8, F and G); however, upregulation of the BCL6 protein in *Mir155*$^{+/+}$ BMDMs was only observed 24 hours after stimulation, whereas BCL6 protein expression was still higher in *Mir155*$^{-/-}$ than in *Mir155*$^{+/+}$ macrophages 6 and 10 hours after stimulation (Figure 8G). Blocking NF-κB activation in *Mir155*$^{+/+}$ BMDMs reduced the expression of *Bcl6* mRNA 24 hours after stimulation with moxLDL and IFN-γ (Figure 8H), which indicates that upregulation via NF-κB activation offsets the suppressive effect of miR-155 on *Bcl6* expression at later stages of the inflammatory macrophage response.

Role of BCL6 in miR-155–mediated protection against atherogenesis. To investigate the role of BCL6 in protection against atherosclerosis in mice harboring *Mir155*$^{-/-}$ BM cells, we analyzed BCL6 expression in lesional macrophages using a combined immunostaining approach (Figure 9A). The number of BCL6-expressing macrophages was substantially increased in *Mir155*$^{+/+}$*Apoe*$^{-/-}$ mice harboring *Mir155*$^{-/-}$*Apoe*$^{-/-}$ BM compared with *Mir155*$^{+/+}$*Apoe*$^{-/-}$ and *Mir155*$^{-/-}$*Apoe*$^{-/-}$ mice harboring *Mir155*$^{+/+}$*Apoe*$^{-/-}$ BM (Figure 9B). Furthermore, *Bcl6* mRNA expression was higher in carotid plaques from mice harboring *Mir155*$^{-/-}$ BM than in those from mice with *Mir155*$^{+/+}$ BM (Figure 9C). Next, we studied the effect of increased *Bcl6* expression in *Apoe*$^{-/-}$ mice harboring *Mir155*$^{-/-}$ BM on atherosclerosis by silencing *Bcl6* in the carotid artery after partial ligation (Supplemental Figure 11). Treatment with *Bcl6* siRNA led to a marked increase in plaque formation compared with nonspecific control siRNA, but did not affect the medial area in *Apoe*$^{-/-}$ mice harboring *Mir155*$^{-/-}$ BM (Figure 10A). Whereas the number of macrophages per lesion was substantially higher after treatment with *Bcl6* siRNA, relative macrophage content and macrophage size were unchanged (Figure 10B and Supplemental Figure 12). Lesional SMC content tended to increase after *Bcl6* siRNA treatment (Supplemental Figure 13). Of note, immunostaining of lesions showed more CCL2-expressing *Mir155*$^{-/-}$ macrophages in arteries treated with *Bcl6* siRNA than with control siRNA (Figure 10C).

Discussion

Chronic, nonresolving inflammation driven by lipid-laden macrophages is crucial for atherosclerotic lesion formation. Here, we found that miR-155 promoted the inflammatory response of macrophages during atherosclerosis. Expression of miR-155 in unstimulated macrophages was essential for the upregulation of CCL2 after inflammatory stimulation by direct suppression of *Bcl6* expression. Thus, miR-155 sensitized macrophages to inflammatory activation by abrogating BCL6-mediated inhibition of NF-κB signaling. The absence of miR-155 in macrophages limited atherosclerotic plaque formation by upregulating *Bcl6*, which decreased the expression of CCL2 in lesional macrophages. Therefore, priming of macrophages for inflammatory activation by miR-155 supported the development of advanced atherosclerotic lesions.

miRs play a crucial role in cell fate transitions and regulate the development and function of immune cells (47). Accordingly, macrophage polarization to inflammatory M1 — and alternatively activated M2 — subtypes is associated with the differential regulation of a distinct set of miRs (29). Upregulation of miR-155 and miR-147 was observed in macrophages upon stimulation of TLRs and after polarization into an M1-type (29, 30, 48); however, the functional roles of these 2 miRs in macrophages differ substantially. Whereas miR-155 primarily enhances proinflammatory cytokine expression, miR-147 is part of a negative feedback loop that constrains the inflammatory response (29, 30, 33). Our present results demonstrated that increased miR-155 and miR-147 expression was characteristic not only of M1-type

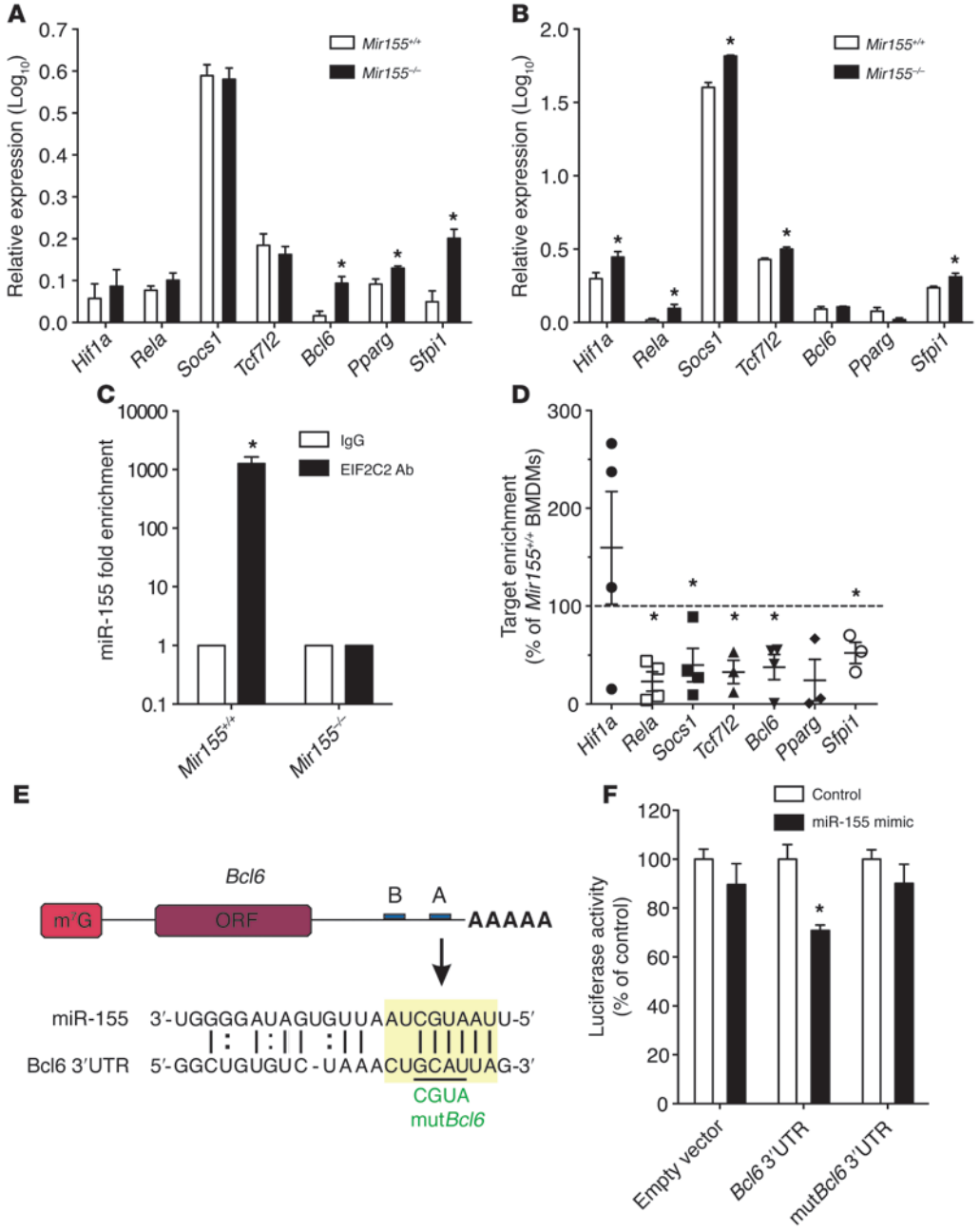

Figure 6

Identification of miR-155 targets in BMDMs. (**A** and **B**) Effect of *Mir155* deficiency on expression of potential miR-155 targets *Hif1a* ($n = 4$) and *Rela*, *Socs1*, *Tcf7l2*, *Bcl6*, *Pparg*, and *Sfpi1* ($n = 3$ for each) in unstimulated (**A**) and moxLDL- and IFN-γ–stimulated (**B**) BMDMs. *$P < 0.05$ vs. *Mir155*$^{+/+}$. (**C**) Quantitative RT-PCR of miR-155 in immunoprecipitates from moxLDL- and IFN-γ–stimulated *Mir155*$^{+/+}$ and *Mir155*$^{-/-}$ BMDMs. Precipitates were obtained after incubation of cell lysates with an anti-EIF2C2 or nonspecific IgG control antibody ($n = 4$ independent experiments per group). *$P < 0.05$ vs. IgG. (**D**) Enrichment of potential miR-155 targets in EIF2C2-IP from moxLDL/IFN-γ–stimulated *Mir155*$^{+/+}$ and *Mir155*$^{-/-}$ BMDMs by quantitative RT-PCR ($n = 3$–4 independent experiments per group). Results are expressed as target enrichment in *Mir155*$^{-/-}$ BMDMs normalized to that in *Mir155*$^{+/+}$ BMDMs. *$P < 0.05$ vs. *Mir155*$^{+/+}$. (**E**) Potential target sites for miR-155 in the 3′UTR of murine *Bcl6* mRNA, as predicted by the miRanda prediction algorithm (sites A and B; blue). Target site A (sequence highlighted in green) was mutated in the binding region. The same sites in the human *Bcl6* 3′UTR are also predicted binding sites for human miR-155, differing from mouse miR-155 by 1 nucleotide. (**F**) Luciferase reporter assays in HEK293 cells treated with miR-155 mimics or nontargeting control mimics using the pEZX-MT01 vector containing the *Bcl6* 3′UTR or the *Bcl6* 3′UTR with mutations in predicted miR-155 binding site A ($n = 3$ independent experiments per group). *$P < 0.05$ vs. control. Data are mean ± SEM.

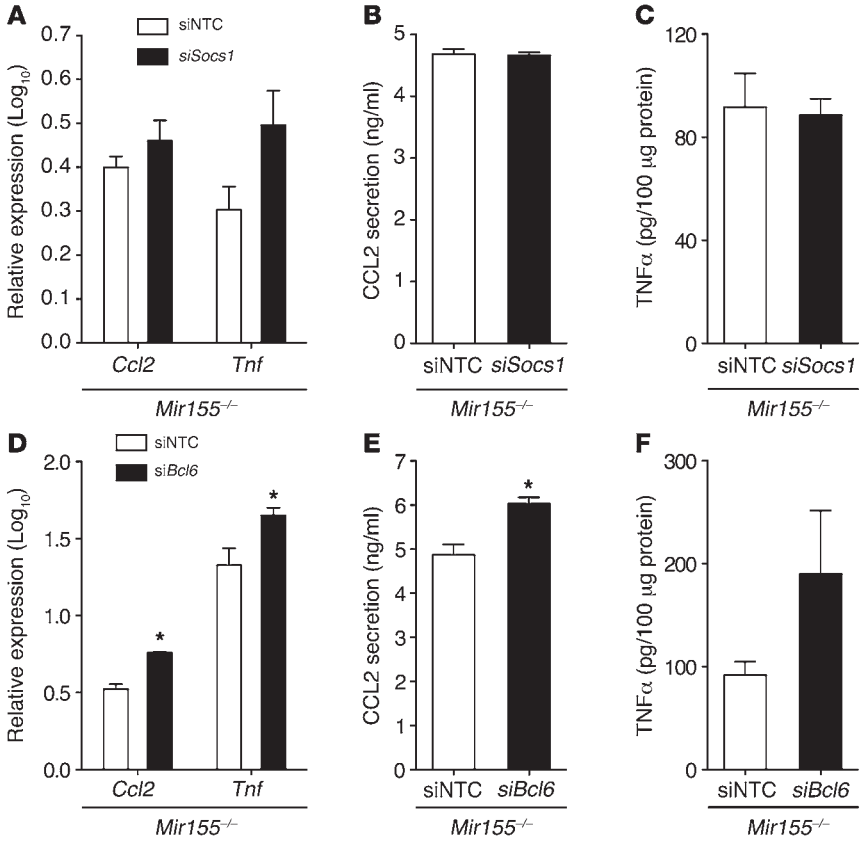

Figure 7
Targeting *Bcl6* mediates the proinflammatory effects of miR-155. (**A**) Effect of siRNA-mediated silencing of *Socs1* (si*Socs1*) in *Mir155*$^{-/-}$ BMDMs on *Ccl2* ($n = 3$) and *Tnf* ($n = 3$) mRNA expression was compared with that mediated by nontargeting control siRNA (siNTC) by quantitative RT-PCR. (**B** and **C**) CCL2 secretion (**B**; $n = 3$) and TNF-α protein expression (**C**; $n = 3$) in *Mir155*$^{-/-}$ BMDMs, compared with that of control siRNA, determined by ELISA. (**D**) Expression of *Ccl2* ($n = 3$) and *Tnf* ($n = 4$) mRNA after siRNA-mediated silencing of *Bcl6* (si*Bcl6*) in *Mir155*$^{-/-}$ BMDMs, compared with that after control siRNA treatment, determined by quantitative RT-PCR. (**E** and **F**) Effect of *Bcl6* siRNA treatment on CCL2 (**E**; $n = 3$) and TNF-α (**F**; $n = 3$) protein expression in *Mir155*$^{-/-}$ BMDMs, compared with that by control siRNA. *$P < 0.05$ vs. control. Data are mean ± SEM.

macrophages, but also of atherosclerotic plaques. In addition to miR-155 and miR-147, 7 miRs — including miR-21, miR-21*, miR-34a, and miR-146a/b, which were upregulated in flow-induced carotid lesions in *Apoe*$^{-/-}$ mice — are also increased in human atherosclerotic plaques (38, 39). Whereas miR-147 expression was also upregulated by hyperlipidemia in the walls of non-atherosclerotic arteries, increased expression of miR-155 was confined to atherosclerotic plaques, which indicates that miR-155 may affect atherosclerosis through its effects on atherogenic macrophages. Although a subset of SMCs in atherosclerotic lesions expressed miR-155, we confirmed that lesional macrophages were an abundant source of miR-155.

In LPS-stimulated macrophages, AKT1-mediated suppression of miR-155 is crucial for the development of endotoxin tolerance and dampening of M1-type macrophage polarization (33, 43). The proinflammatory role of miR-155 is associated with targeting inhibitors of cytokine signalling, such as *Socs1* or *Inpp5d* (33, 49). In addition, the antiinflammatory effect of IL-10 on macrophages has previously been linked to the inhibition of miR-155 transcription, resulting in increased expression of *Inpp5d* (50). However, suppression of inflammatory cytokines (such as IL-1β and TNF-α) and of NF-κB activity by miR-155 was described in monocyte-derived dendritic cells and oxLDL-treated THP-1 macrophages (51). The results of the present study clearly showed that miR-155 promoted the proinflammatory activation of macrophages by enhancing the expression of *Ccl2* and *Tnf*. Although we found that confirmed miR-155 targets in inflammatory macrophages, such as *Socs1*, were indeed targeted by miR-155, the direct effects of miR-155 on *Ccl2* and *Tnf* expression were mediated by suppression of *Bcl6*. Therefore, our results demonstrated that targeting of the transcriptional repressor *Bcl6* by miR-155 is a key mechanism underlying the inflammatory activation of macrophages.

Accordingly, we found that targeting of *Bcl6* by miR-155 in unstimulated macrophages promoted subsequent proinflammatory activation. However, once fully activated, the suppressive effect of miR-155 was offset by the NF-κB–mediated upregulation of *Bcl6*, which may be important for the resolution of the inflammatory response. Thus, our data suggest that miR-155–mediated suppression of *Bcl6* is crucial for the acute inflammatory activation of macrophages, whereas feedback inhibition through NF-κB–induced *Bcl6* expression prevails during the postactivation state.

We also found that deficiency of miR-155 in hematopoietic cells, but not in vascular cells, attenuated advanced atherosclerosis induced by acute flow disturbance and hyperlipidemia via increased BCL6 expression by macrophages. The reduction in lesion size observed in mice harboring *Mir155*$^{-/-}$ BM was due to fewer macrophages in the plaques. Upregulation of BCL6 in lesional *Mir155*$^{-/-}$ macrophages repressed CCL2 expression, which is known to promote the recruitment of monocytes to atherosclerotic plaques (18). In addition to its immunoregulatory functions, miR-155 can enhance or prevent the apoptosis of infected macrophages (52, 53). However, we did not observe any effect of miR-155 on the apoptosis of lesional macrophages. In contrast to our findings, increased HFD-induced early atherosclerosis and neutrophil infiltration into lesions was described in *Ldlr*$^{-/-}$ mice harboring *Mir155*$^{-/-}$ BM (54). Neutrophils primarily play a role during early atherogenesis by enhancing the recruitment of monocytes, whereas advanced atherosclerosis appears to be less

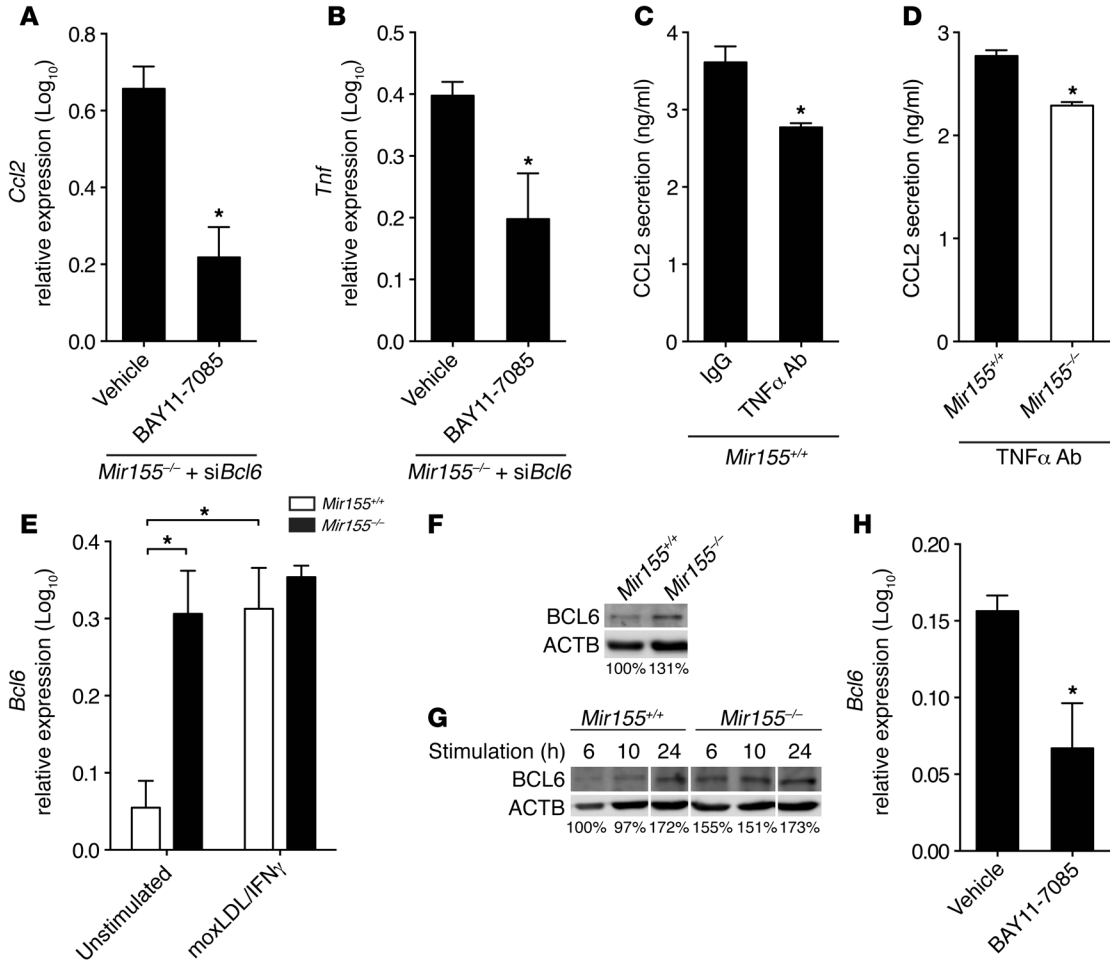

Figure 8

Role of NF-κB and TNF-α in regulating CCL2 and BCL6 expression during macrophage stimulation. (**A** and **B**) Role of NF-κB signaling in increased *Ccl2* (**A**) and *Tnf* (**B**) mRNA expression in *Bcl6* siRNA–treated *Mir155*$^{-/-}$ BMDMs, as determined using the NF-κB inhibitor BAY11-7085. (**C**) CCL2 protein levels in the medium of *Mir155*$^{+/+}$ BMDMs after stimulation with moxLDL and IFN-γ, quantified by ELISA. A blocking antibody against TNF-α or an isotype control antibody was added to the medium. (**D**) CCL2 protein levels in the medium of *Mir155*$^{+/+}$ or *Mir155*$^{-/-}$ BMDMs after stimulation with moxLDL and IFN-γ, quantified by ELISA. A blocking antibody against TNF-α (5 μg/ml) was added to the medium in both groups. (**E**) Effect of moxLDL and IFN-γ stimulation on *Bcl6* mRNA expression in *Mir155*$^{+/+}$ and *Mir155*$^{-/-}$ BMDMs. (**F**) BCL6 protein expression in unstimulated *Mir155*$^{+/+}$ and *Mir155*$^{-/-}$ BMDMs, determined by Western blot. (**G**) Time course of BCL6 protein expression after moxLDL and IFN-γ stimulation of *Mir155*$^{+/+}$ and *Mir155*$^{-/-}$ BMDMs, determined by Western blot. The intensity of the BCL6 bands relative to that of ACTB bands is expressed as a percentage of that in unstimulated BMBMs (**F**) or in *Mir155*$^{+/+}$ BMDMs 6 hours after stimulation (**G**). Lanes in **G** were run on the same gel but were noncontiguous (white lines). (**H**) *Bcl6* mRNA expression in BMDMs stimulated with moxLDL and IFN-γ after treatment with BAY11-7085 or vehicle. *$P < 0.05$. $n = 3$ independent experiments per group. Data are mean ± SEM.

influenced by neutrophils (55). Accordingly, we did not observe any effect of miR-155 on the neutrophil content of advanced carotid lesion that were induced by disturbed flow, which suggests that miR-155 affects atherosclerosis in a stage-dependent manner. In contrast to early atherosclerosis, in which *Mir155* deficiency disturbs neutrophil homeostasis, the proinflammatory role of miR-155 in macrophage activation promoted advanced atherosclerosis. In line with our results, *Bcl6* deficiency in BM cells from *Ldlr*$^{-/-}$ mice exacerbates atherosclerosis and increases the expression of genes involved in atherogenic inflammation, such as CCL2 (56). Taken together, our findings suggest that miR-155–mediated suppression of *Bcl6* sensitizes macrophages to atherogenic activation and that this is a key inflammatory mechanism in advanced atherosclerosis.

In addition to upregulating miR-155 in inflammatory macrophages, we found that both native LDL and moxLDL increased the expression of miR-155, although to a lesser extent than did LPS and IFN-γ. In contrast, profoundly oxLDL suppressed the expression of miR-155 in macrophages. Previous results from studies of the effects of oxLDL on miR-155 expression are conflicting. For example, both up- and downregulation of miR-155 in response to oxLDL has been reported in THP-1 macrophages (34, 37). Moreover, treatment with oxLDL can induce the expression of miR-155 in human primary monocytes (36). According to our present results, regulation of miR-155 expression depended on the level of oxLDL modification, which may explain the controversial findings previously reported in the literature. Interestingly, higher levels of LDL oxidation inhibited both the expression of

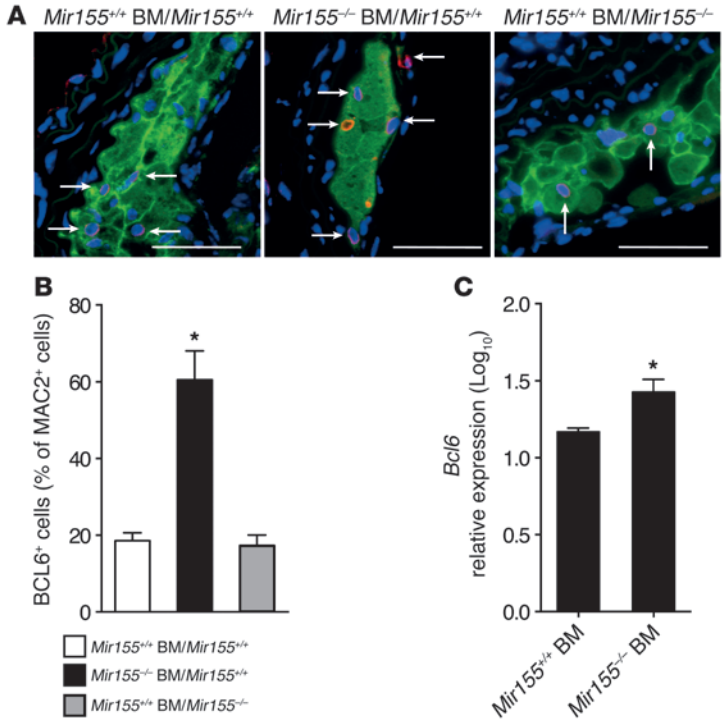

Figure 9
Expression of lesional BCL6 is miR-155 dependent. (**A**) Combined immunostaining for Bcl6 (red) and MAC2 (green) in atherosclerotic lesions of carotid arteries after partial ligation in *Mir155*$^{+/+}$*Apoe*$^{-/-}$ mice harboring *Mir155*$^{+/+}$*Apoe*$^{-/-}$ or *Mir155*$^{-/-}$*Apoe*$^{-/-}$ BM and in *Mir155*$^{-/-}$*Apoe*$^{-/-}$ mice harboring *Mir155*$^{+/+}$*Apoe*$^{-/-}$ BM. Representative images are shown. Nuclei were counterstained with DAPI (blue). Arrows denote BCL6-expressing macrophages. Scale bars: 50 μm. (**B**) BCL6^{+} macrophages in sections of carotid lesions immunostained for BCL6 and MAC2 (n = 6–8 per group). (**C**) *Bcl6* mRNA expression in lesions of carotid arteries 6 weeks after partial ligation in *Mir155*$^{+/+}$*Apoe*$^{-/-}$ mice harboring *Mir155*$^{+/+}$*Apoe*$^{-/-}$ or *Mir155*$^{-/-}$*Apoe*$^{-/-}$ BM, determined by quantitative RT-PCR (n = 4 per group). *P < 0.05. Data are mean ± SEM.

inflammatory cytokines in macrophages and the activation of NF-κB, which is essential for the transcriptional upregulation of miR-155 (57–59). In addition to the regulation of miR-155 in macrophages by modified LDL, we found that lesional *Mir155*$^{-/-}$ macrophages accumulated fewer lipids. This is in contrast to previous in vitro results, which report increased lipid accumulation in THP-1 macrophages following treatment with a miR-155 inhibitor (37). Interestingly, the expression of PPARγ, which plays a key role in the alternative activation and effective lipid handling of macrophages (including LDL uptake and cholesterol efflux), was increased in *Mir155*$^{-/-}$ macrophages (10). Although our results do not indicate that miR-155 targets PPARγ in inflammatory macrophages, miR-155 suppressed PPARγ in unstimulated macrophages, which express much higher levels of PPARγ than do inflammatory macrophages (60). Alternatively, PPARγ levels might be reduced indirectly in miR-155–expressing macrophages via enhanced NF-κB activation (60, 61). Despite the reduced lipid accumulation in *Mir155*$^{-/-}$ lesional macrophages, the size of the macrophages in atherosclerotic lesions was not altered by *Mir155* deficiency. Therefore, we conclude that differences in lipid accumulation are not caused by reduced lesion formation in mice harboring *Mir155*$^{-/-}$ macrophages.

In summary, we showed that increased miR-155 expression in proinflammatory macrophages promoted atherosclerosis by derepressing BCL6-mediated inhibition of CCL2 transcription. We therefore conclude that miR-155 plays a key role in the atherogenic programming of macrophages, which sustains and amplifies vascular inflammation.

Methods

See Supplemental Methods for details regarding human carotid plaque sample collection, micro–computed tomography, quantitative RT-PCR, moxLDL preparation, cell culture, migration and apoptosis assays, miR-155 target gene prediction, Western blot analysis, ELISA, and lipoprotein profiling.

Animal models of atherosclerosis. Female *Apoe*$^{-/-}$ mice (6–8 weeks old; Jackson Laboratory) were fed HFD (21% crude fat, 0.15% cholesterol, 19.5% casein; Altromin) for 3 or 10 months. The aorta was then harvested after in situ perfusion with RNAlater (Ambion) via the left ventricle. For the control group, arteries were collected from female *Apoe*$^{-/-}$ mice (8 weeks old) fed regular chow diet.

Mir155$^{-/-}$ mice (Jackson Laboratory) were crossed with *Apoe*$^{-/-}$ mice to obtain double-deficient *Mir155*$^{-/-}$*Apoe*$^{-/-}$ mice. BM cells from *Mir155*$^{+/+}$*Apoe*$^{-/-}$ and *Mir155*$^{-/-}$*Apoe*$^{-/-}$ mice (5–10 × 10^{6} cells) were injected into the tail vein of *Mir155*$^{+/+}$*Apoe*$^{-/-}$ recipients treated with an ablative dose of whole-body irradiation (2 × 6.5 Gy). In HFD-fed mice, atherosclerotic plaques were induced 4 weeks after BM transplantation by partial carotid ligation (41). In brief, mice were anesthetized with ketamin and xylazine, and the left external carotid, internal carotid, and occipital arteries were ligated. This partial carotid ligation resulted in acutely reduced blood flow velocity in the common carotid artery due to restricted outflow through the superior thyroid artery. Perivascular treatment of the carotid artery with *Bcl6* siRNA (Accell siRNA, 4 nmol/treatment; Dharmacon) was performed once weekly starting 2 weeks after partial ligation. In the control group, the partially ligated carotid arteries were treated with nontargeting siRNA (Dharmacon). The siRNA was mixed with transfection reagent (DharmaFECT 4; Dharmacon) and dissolved in pluronic gel (35%; Sigma-Aldrich) as described previously (19). The left and right carotid arteries were harvested 6 weeks after partial ligation following in situ perfusion with RNAlater (Ambion), paraformaldehyde, or PAXgene Tissue Fix (PAXgene Tissue Containers; Qiagen) through the left ventricle.

Laser capture microdissection. Serial sections (20 μm thick) of the carotid and innominate arteries and the aortic root were mounted on membrane-mounted metal frame slides (Molecular Machines and Industries), deparaffinized under RNase-free conditions, and completely dried. Laser capture microdissection was performed using a laser microdissection system (MMI cellcut plus; Molecular Machines and Industries) attached to an inverted microscope (IX71; Olympus). At least 40 sections of plaque tissue or morphologically normal vessel wall tissue were collected from each mouse. RNA was isolated using the RecoverAll total nucleic acid isolation kit (Life Technologies) according to the manufacturer's instructions.

miR real-time PCR array. Total RNA was isolated from carotid arteries and cultured BMDMs using the mirVana kit (Invitrogen), and the quality of the RNA was determined using an Agilent 2100 Bioanalyzer. Reverse transcription and preamplification was performed using the Megaplex RT & Preamp Rodent Pool Set (Life Technologies) according to the manufacturer's instructions. Samples were loaded onto preconfigured 384-well microfluidic cards (TaqMan Array MicroRNA Cards) for real-time analysis of 518 mouse miRs (Sanger miRBase v10) using a 7900HT RT-PCR System (Life Technologies). Data were analyzed using StatMiner software

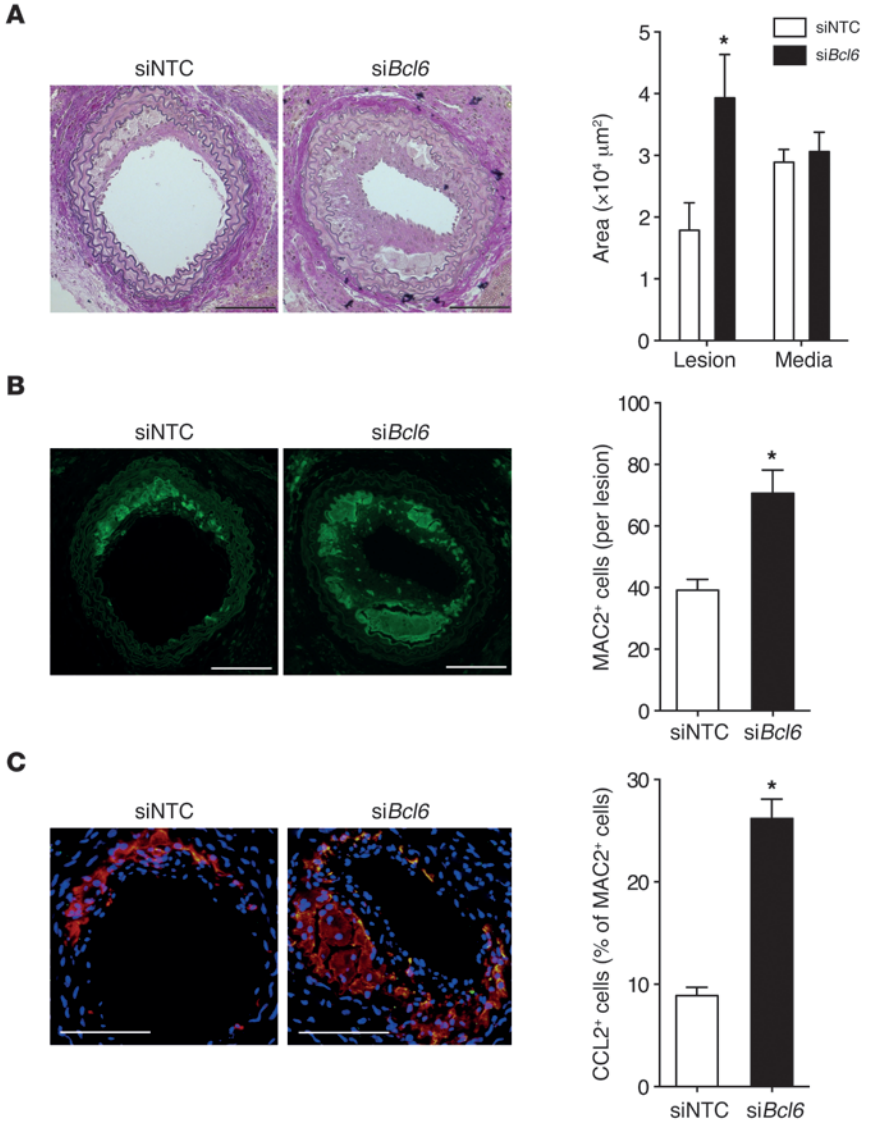

Figure 10
Role of BCL6 in miR-155–mediated atherosclerosis. Partially ligated carotid arteries from *Apoe*$^{-/-}$ mice harboring *Mir155*$^{-/-}$ BM were perivascularly treated with *Bcl6* siRNA or nontargeting control siRNA. (**A**) Lesion area and medial area were determined in carotid artery sections stained with EVG by planimetry. Representative images are shown. (**B**) Number of macrophages in lesions from the carotid artery, analyzed by immunostaining for MAC2 (green). Representative images are shown, and the number of MAC2$^+$ cells per lesion was determined. (**C**) Combined immunostaining for CCL2 (green) and MAC2 (red) was performed in carotid artery sections, and the percentage of CCL2$^+$ macrophages (yellow) was quantified. n = 4–5 per group. *P < 0.05. Scale bars: 100 μm. Data are mean ± SEM.

(Integromics) according to the ΔΔCt method using multiple internal control genes. The most stable combination of internal controls was determined using the Genorm algorithm. A Ct value less than 40 was defined as the limit of detection of the individual assays. The fold change compared with the control group was calculated and logarithmically transformed (log_{10}). Array data were deposited in GEO (http://www.ncbi.nlm.nih.gov/geo/; accession nos. GSE26555 and GSE33453).

Immunostaining and histology. Serial sections (5 μm thick) from the common carotid artery were collected within 1 mm of the area of bifurcation and stained (3–5 sections per mouse) with elastic van Gieson (EVG) stain. Images were obtained under a brightfield microscope (Leica DMLB) connected to a CCD camera (JVC). The plaque area was quantified by planimetry (Diskus software; Hilgers, Bonn).

Quantitative immunostaining for TAGLN (rabbit polyclonal; Abcam); SMA, MAC2, and CD3E (rabbit polyclonal; Dako); MPO (rabbit polyclonal; Abcam); and collagen type I (rabbit polyclonal; Cedarlane) was performed on carotid artery sections. The primary antibody was detected with a fluorescently labeled secondary antibody. The percentage of positively stained area per total plaque area (2–3 sections/mouse, 50- to 100-μm distance between sections) was determined using image analysis software (ImageJ), with the threshold set according to the background of negative control staining. Combined immunostaining for CCL2/MAC2 or BCL6/MAC2 was performed by sequential incubation of the carotid sections with either an anti-CCL2 antibody (goat polyclonal; Santa Cruz Biotechnology) or an anti-BCL6 antibody (rabbit polyclonal; Abcam) followed by a FITC-labeled secondary antibody and an anti-MAC2 antibody, which was visualized using a Dylight549-conjugated anti-rat antibody (KPL).

Combined in situ hybridization and immunostaining. Sections (7 μm thick) from carotid arteries fixed with Paxgene (Qiagen) were hybridized with double digoxigenin-labeled probes (miR-155 and scrambled probes, 50 nM; *U6* probe, 5 nM) in hybridization buffer (Exiqon) at 51°C for 1 hour in a Thermoblock (Eppendorf). After stringent washing with SSC buffer and blockade of nonspecific binding sites using TNB (Perkin Elmer) and biotin/avidin binding sites using a blocking kit (Vector Lab), sections were incubated with a peroxidase-conjugated anti-digoxigenin antibody (Fab fragments from sheep, 1:100 dilution; Roche) for 1 hour at 37°C. A tyramide-based amplification system (TSA Plus Biotin; Perkin Elmer) and Dylight 549–conjugated streptavidin (KPL) were used to visualize the probe. Sections were subsequently incubated with anti-MAC2 (rat, clone M3/38; Cederlane) or anti-SMA (mouse, clone1A4; Dako) antibodies followed by a FITC-conjugated secondary antibody.

EIF2C2 IP. BMDMs from *Mir155*$^{+/+}$*Apoe*$^{-/-}$ and *Mir155*$^{-/-}$*Apoe*$^{-/-}$ mice were washed in ice-cold PBS and incubated with lysis buffer (100 mM KCl, 5 mM $MgCl_2$, 10 mM HEPES [pH 7.0], 0.5% NP40, 5 mM DTT, 250 U/ml RNase OUT [Invitrogen], 400 μM vanadyl ribonucleoside complexes [New England Biolabs], and protease inhibitors [Complete Protease Inhibitor Cocktail Tablets; Roche]) for 15 minutes on ice. After homogenization in a Dounce homogenizer, cell extracts were centrifuged. Input RNA was extracted from the supernatant using TRIzol (Invitrogen). Before IP, protein A/G conjugated to magnetic beads (Millipore) was incubated with a mouse monoclonal anti-EIF2C2 antibody (clone 2E12-1C9; Abnova) or mouse IgG (Millipore). The antibody-conjugated beads were then incubated with the cell extracts for 5 hours at 4°C before immobilization of the precipitate with

a magnetic separator (Millipore). RNA was isolated from the precipitate with TRIzol, reverse transcribed with random primers, and amplified using the SYBR Green PCR Master Mix (Fermentas). The fold enrichment (FE) of target genes in the EIF2C2-IP RNA compared with that in IgG-IP RNA was determined as follows: (a) $\Delta Ct_{EIF2C2\text{-}IP}$ was calculated as $Ct_{input} - Ct_{EIF2C2\text{-}IP}$; (b) $\Delta Ct_{IgG\text{-}IP}$ was calculated as $Ct_{input} - Ct_{IgG\text{-}IP}$; (c) $\Delta\Delta Ct$ was calculated as $\Delta Ct_{EIF2C2\text{-}IP} - \Delta Ct_{IgG\text{-}IP}$; and (d) FE was calculated as $2^{\Delta\Delta Ct}$.

Luciferase assay. Constructs of the pEZX-MT01 vector with or without the 3′UTR of the murine *Bcl6* gene were purchased from GeneCopoeia. Mutagenesis PCR was performed at the miR-155 target site of *Bcl6*. HEK293 cells were transfected with 100 ng luciferase reporter or empty vector and treated with miR-155 mimic (30 nM, Ambion Pre-miR miRNA Precusor; Life Technologies) or nontargeting control oligonucleotides (30 nM, Pre-miR miRNA Precusor Negative Control) using Lipofectamine 2000 (Invitrogen). Firefly and Renilla luciferase activity were assessed using the Dual-Glo Luciferase Assay System (Promega) and a microplate reader (Tecan) 72 hours after transfection.

Statistics. miR array data are presented as means and were compared using unpaired, moderated, 2-tailed *t* test (Statminer 4.2; Integromics). A false-positive discovery test (according to the Benjamini-Hochberg procedure) was applied to the array data. All other data represent mean ± SEM. 2 groups were compared using paired, 2-tailed *t* test; more than 2 groups were compared using 1-way ANOVA followed by Newman-Keuls post-test (Prism 5.0; GraphPad). A *P* value less than 0.05 was considered significant.

Study approval. Animal experiments were reviewed and approved by the local authorities (LANUV NRW) in accordance with German animal protection laws. The Ethics Committee of the Medical Faculty (RWTH Aachen University) approved the study protocol for the collection of human atherosclerotic plaque samples, and written informed consent was obtained from all participating subjects.

Acknowledgments

This work was supported by the DFG (Scho1056/3-1 and FOR809), by the Interdisciplinary Centre for Clinical Research within the Faculty of Medicine at the RWTH Aachen University (to M. Nazari-Jahantigh), and by the German Centre for Cardiovascular Research (MHA VD 1.2). We thank Anna Thiemann, Stephanie Wilbertz, Melanie Garbe, and Roya Soltan for technical assistance and Pallavi Subramanian for assistance in analyzing immunostainings.

Received for publication November 3, 2011, and accepted in revised form August 20, 2012.

Address correspondence to: Andreas Schober, Institute for Cardiovascular Prevention, Ludwig-Maximilians University Munich, Pettenkoferstr. 9, 80336 Munich, Germany. Phone: 49.89.51605151; Fax: 49.89.51604740; E-mail: aschober@med.lmu.de.

1. Moore KJ, Tabas I. Macrophages in the pathogenesis of atherosclerosis. *Cell*. 2011;145(3):341–355.
2. Weber C, Noels H. Atherosclerosis: current pathogenesis and therapeutic options. *Nat Med*. 2011; 17(11):1410–1422.
3. Zhao Y, Van Berkel TJ, Van Eck M. Relative roles of various efflux pathways in net cholesterol efflux from macrophage foam cells in atherosclerotic lesions. *Curr Opin Lipidol*. 2010;21(5):441–453.
4. Marcel YL, Ouimet M, Wang M-D. Regulation of cholesterol efflux from macrophages. *Curr Opin Lipidol*. 2008;19(5):455–461.
5. Ouimet M, Marcel YL. Regulation of lipid droplet cholesterol efflux from macrophage foam cells. *Arterioscler Thromb Vasc Biol*. 2012;32(3):575–581.
6. Ricote M, Li AC, Willson TM, Kelly CJ, Glass CK. The peroxisome proliferator-activated receptor-gamma is a negative regulator of macrophage activation. *Nature*. 1998;391(6662):79–82.
7. Li Y, Tabas I. The inflammatory cytokine response of cholesterol-enriched macrophages is dampened by stimulated pinocytosis. *J Leukoc Biol*. 2007; 81(2):483–491.
8. Duewell P, et al. NLRP3 inflammasomes are required for atherogenesis and activated by cholesterol crystals. *Nature*. 2010;464(7293):1357–1361.
9. Li Y, et al. Free cholesterol-loaded macrophages are an abundant source of tumor necrosis factor-alpha and interleukin-6: model of NF-kappaB- and map kinase-dependent inflammation in advanced atherosclerosis. *J Biol Chem*. 2005; 280(23):21763–21772.
10. Ricote M, Valledor AF, Glass CK. Decoding transcriptional programs regulated by PPARs and LXRs in the macrophage: effects on lipid homeostasis, inflammation, and atherosclerosis. *Arterioscler Thromb Vasc Biol*. 2004;24(2):230–239.
11. McGillicuddy FC, et al. Inflammation impairs reverse cholesterol transport in vivo. *Circulation*. 2009;119(8):1135–1145.
12. Miller YI, Choi SH, Fang L, Harkewicz R. Toll-like receptor-4 and lipoprotein accumulation in macrophages. *Trends Cardiovasc Med*. 2009;19(7):227–232.
13. Kanters E, et al. Hematopoietic NF-kappaB1 deficiency results in small atherosclerotic lesions with an inflammatory phenotype. *Blood*. 2004;103(3):934–940.
14. Vallabhapurapu S, Karin M. Regulation and function of NF-kappaB transcription factors in the immune system. *Annu Rev Immunol*. 2009; 27:693–733.
15. Kanters E, et al. Inhibition of NF-kappaB activation in macrophages increases atherosclerosis in LDL receptor-deficient mice. *J Clin Invest*. 2003; 112(8):1176–1185.
16. Björkbacka H, et al. Reduced atherosclerosis in MyD88-null mice links elevated serum cholesterol levels to activation of innate immunity signaling pathways. *Nat Med*. 2004;10(4):416–421.
17. Michelsen KS, et al. Lack of Toll-like receptor 4 or myeloid differentiation factor 88 reduces atherosclerosis and alters plaque phenotype in mice deficient in apolipoprotein E. *Proc Natl Acad Sci U S A*. 2004;101(29):10679–10684.
18. Aiello RJ, et al. Monocyte chemoattractant protein-1 accelerates atherosclerosis in apolipoprotein E-deficient mice. *Arterioscler Thromb Vasc Biol*. 1999; 19(6):1518–1525.
19. Zhou Z, et al. Lipoprotein-derived lysophosphatidic acid promotes atherosclerosis by releasing CXCL1 from the endothelium. *Cell Metab*. 2011; 13(5):592–600.
20. Ci W, Polo JM, Melnick A. B-cell lymphoma 6 and the molecular pathogenesis of diffuse large B-cell lymphoma. *Curr Opin Hematol*. 2008;15(4):381–390.
21. Li Z, et al. BCL-6 negatively regulates expression of the NF-kappaB1 p105/p50 subunit. *J Immunol*. 2005;174(1):205–214.
22. Perez-Rosado A, Artiga M, Vargiu P, Sanchez-Aguilera A, Alvarez-Barrientos A, Piris M. BCL6 represses NFkappaB activity in diffuse large B-cell lymphomas. *J Pathol*. 2008;214(4):498–507.
23. Barish GD, et al. Bcl-6 and NF-kappaB cistromes mediate opposing regulation of the innate immune response. *Genes Dev*. 2010;24(24):2760–2765.
24. Toney LM, et al. BCL-6 regulates chemokine gene transcription in macrophages. *Nat Immunol*. 2000;1(3):214–220.
25. O'Connell RM, Zhao JL, Rao DS. MicroRNA function in myeloid biology. *Blood*. 2011;118(11):2960–2969.
26. Baek D, Villén J, Shin C, Camargo FD, Gygi SP, Bartel DP. The impact of microRNAs on protein output. *Nature*. 2008;455(7209):64–71.
27. Bartel DP. MicroRNAs: target recognition and regulatory functions. *Cell*. 2009;136(2):215–233.
28. Qi J, Qiao Y, Wang P, Li S, Zhao W, Gao C. microRNA-210 negatively regulates LPS-induced production of proinflammatory cytokines by targeting NF-kappaB1 in murine macrophages. *FEBS Lett*. 2012; 586(8):1201–1207.
29. Graff JW, Dickson AM, Clay G, McCaffrey AP, Wilson ME. Identifying functional microRNAs in macrophages with polarized phenotypes. *J Biol Chem*. 2012;287(26):21816–21825.
30. Liu G, Friggeri A, Yang Y, Park YJ, Tsuruta Y, Abraham E. miR-147, a microRNA that is induced upon Toll-like receptor stimulation, regulates murine macrophage inflammatory responses. *Proc Natl Acad Sci U S A*. 2009;106(37):15819–15824.
31. Taganov KD, Boldin MP, Chang KJ, Baltimore D. NF-kappaB-dependent induction of microRNA miR-146, an inhibitor targeted to signaling proteins of innate immune responses. *Proc Natl Acad Sci U S A*. 2006;103(33):12481–12486.
32. O'Neill LA, Sheedy FJ, McCoy CE. MicroRNAs: the fine-tuners of Toll-like receptor signalling. *Nat Rev Immunol*. 2011;11(3):163–175.
33. Androulidaki A, et al. The kinase Akt1 controls macrophage response to lipopolysaccharide by regulating microRNAs. *Immunity*. 2009;31(2):220–231.
34. Yang K, et al. MiR-146a inhibits oxidized low-density lipoprotein-induced lipid accumulation and inflammatory response via targeting toll-like receptor 4. *FEBS Lett*. 2011;585(6):854–860.
35. Nazari-Jahantigh M, Wei Y, Schober A. The role of microRNAs in arterial remodelling. *Thromb Haemost*. 2012;107(4):611–618.
36. Chen T, et al. MicroRNA-125a-5p partly regulates the inflammatory response, lipid uptake, and ORP9 expression in oxLDL-stimulated monocyte/macrophages. *Cardiovasc Res*. 2009;83(1):131–139.
37. Huang RS, Hu GQ, Lin B, Lin ZY, Sun CC. MicroRNA-155 silencing enhances inflammatory response and lipid uptake in oxidized low-density lipoprotein-stimulated human THP-1 macrophages. *J Investig Med*. 2010;58(8):961–967.
38. Raitoharju E, et al. miR-21, miR-210, miR-34a, and miR-146a/b are up-regulated in human athero-

sclerotic plaques in the Tampere Vascular Study. *Atherosclerosis*. 2011;219(1):211–217.
39. Bidzhekov K, et al. microRNA expression signatures and parallels between monocyte subsets and atherosclerotic plaque in humans. *Thromb Haemost*. 2012;107(4):619–625.
40. Rayner KJ, et al. Antagonism of miR-33 in mice promotes reverse cholesterol transport and regression of atherosclerosis. *J Clin Invest*. 2011; 121(7):2921–2931.
41. Nam D, et al. Partial carotid ligation is a model of acutely induced disturbed flow, leading to rapid endothelial dysfunction and atherosclerosis. *Am J Physiol Heart Circ Physiol*. 2009;297(4):H1535–H1543.
42. Gremse F, et al. Virtual elastic sphere processing enables reproducible quantification of vessel stenosis at CT and MR angiography. *Radiology*. 2011; 260(3):709–717.
43. Arranz A, et al. Akt1 and Akt2 protein kinases differentially contribute to macrophage polarization. *Proc Natl Acad Sci U S A*. 2012;109(24):9517–9522.
44. McLaren JE, Ramji DP. Interferon gamma: a master regulator of atherosclerosis. *Cytokine Growth Factor Rev*. 2009;20(2):125–135.
45. Faraoni I, Antonetti FR, Cardone J, Bonmassar E. miR-155 gene: a typical multifunctional microRNA. *Biochim Biophys Acta*. 2009;1792(6):497–505.
46. Natoli G, Ghisletti S, Barozzi I. The genomic landscapes of inflammation. *Genes Dev*. 2011; 25(2):101–106.
47. O'Connell RM, Rao DS, Chaudhuri AA, Baltimore D. Physiological and pathological roles for microRNAs in the immune system. *Nat Rev Immunol*. 2010; 10(2):111–122.
48. O'Connell RM, Taganov KD, Boldin MP, Cheng G, Baltimore D. MicroRNA-155 is induced during the macrophage inflammatory response. *Proc Natl Acad Sci U S A*. 2007;104(5):1604–1609.
49. Kurowska-Stolarska M, et al. MicroRNA-155 as a proinflammatory regulator in clinical and experimental arthritis. *Proc Natl Acad Sci U S A*. 2011; 108(27):11193–11198.
50. McCoy CE, et al. IL-10 inhibits miR-155 induction by toll-like receptors. *J Biol Chem*. 2010; 285(27):20492–20498.
51. Ceppi M, et al. MicroRNA-155 modulates the interleukin-1 signaling pathway in activated human monocyte-derived dendritic cells. *Proc Natl Acad Sci U S A*. 2009;106(8):2735–2740.
52. Ghorpade DS, Leyland R, Kurowska-Stolarska M, Patil SA, Balaji KN. MicroRNA-155 is required for mycobacterium bovis BCG-mediated apoptosis of macrophages. *Mol Cell Biol*. 2012; 32(12):2239–2253.
53. Koch M, Mollenkopf HJ, Klemm U, Meyer TF. Induction of microRNA-155 is TLR- and type IV secretion system-dependent in macrophages and inhibits DNA-damage induced apoptosis. *Proc Natl Acad Sci U S A*. 2012;109(19):E1153–E1162.
54. Donners MM, et al. Hematopoietic miR155 deficiency enhances atherosclerosis and decreases plaque stability in hyperlipidemic mice. *PLoS One*. 2012;7(4):e35877.
55. Drechsler M, Megens RT, van Zandvoort M, Weber C, Soehnlein O. Hyperlipidemia-triggered neutrophilia promotes early atherosclerosis. *Circulation*. 2010;122(18):1837–1845.
56. Barish GD, et al. The Bcl6-SMRT/NCoR cistrome represses inflammation to attenuate atherosclerosis. *Cell Metab*. 2012;15(4):554–562.
57. Ohlsson BG, et al. Oxidized low density lipoprotein inhibits lipopolysaccharide-induced binding of nuclear factor-kappaB to DNA and the subsequent expression of tumor necrosis factor-alpha and interleukin-1beta in macrophages. *J Clin Invest*. 1996;98(1):78–89.
58. Hamilton TA, Major JA, Chisolm GM. The effects of oxidized low density lipoproteins on inducible mouse macrophage gene expression are gene and stimulus dependent. *J Clin Invest*. 1995; 95(5):2020–2027.
59. Gatto G, Rossi A, Rossi D, Kroening S, Bonatti S, Mallardo M. Epstein-Barr virus latent membrane protein 1 trans-activates miR-155 transcription through the NF-kappaB pathway. *Nucleic Acids Res*. 2008;36(20):6608–6619.
60. Welch JS, Ricote M, Akiyama TE, Gonzalez FJ, Glass CK. PPARgamma and PPARdelta negatively regulate specific subsets of lipopolysaccharide and IFN-gamma target genes in macrophages. *Proc Natl Acad Sci U S A*. 2003;100(11):6712–6717.
61. Necela BM, Su W, Thompson EA. Toll-like receptor 4 mediates cross-talk between peroxisome proliferator-activated receptor gamma and nuclear factor-kappaB in macrophages. *Immunology*. 2008; 125(3):344–358.